

Teacher-Guided Student Self-Knowledge Distillation Using Diffusion Model

Yu Wang^{1,2}, Chuanguang Yang^{1†}, Zhulin An^{1†}, Weilun Feng^{1,2}, Jiarui Zhao^{1,2}, Chengqing Yu¹, Libo Huang¹, Boyu Diao¹, Yongjun Xu¹

¹State Key Laboratory of AI Safety, Institute of Computing Technology, Chinese Academy of Sciences,

²University of Chinese Academy of Sciences

†Corresponding authors

Existing Knowledge Distillation (KD) methods often align feature information between teacher and student by exploring meaningful feature processing and loss functions. However, due to the difference in feature distributions between the teacher and student, the student model may learn incompatible information from the teacher. To address this problem, we propose teacher-guided student **Diffusion Self-KD**, dubbed as DSKD. Instead of the direct teacher-student alignment, we leverage the teacher classifier to guide the sampling process of denoising student features through a light-weight diffusion model. We then propose a novel locality-sensitive hashing (LSH)-guided feature distillation method between the original and denoised student features. The denoised student features encapsulate teacher knowledge and could be regarded as a teacher role. In this way, our DSKD method could eliminate discrepancies in mapping manners and feature distributions between the teacher and student, while learning meaningful knowledge from the teacher. Experiments on visual recognition tasks demonstrate that DSKD significantly outperforms existing KD methods across various models and datasets.



1 Introduction

In the era of deep learning, how to compress large models while maintaining their performance has become a valuable topic. Knowledge Distillation (KD) is a well-known technique to achieve this goal. The core idea of KD is to transfer the knowledge from a pre-trained, high-capacity teacher network to a lightweight student network. With additional teacher guidance, the student performance could be significantly improved compared to training independently.

The original KD [Hinton et al. \(2015\)](#) guides the student to learn from the teacher's final class probability predictions by KL divergence. This intuitive idea helps the student mimic the teacher's better outputs effectively. However, the final predictions lack intermediate information, making the student unable to understand the teacher's thinking process. Therefore, many works explore feature distillation methods that distill intermediate feature maps [Romero et al. \(2014\)](#) or their extracted information [Zagoruyko and Komodakis \(2016\)](#); [Wang et al. \(2021\)](#). The reason behind the success of feature distillation is that intermediate features encode the comprehensive information during the inference process.

However, these methods share a common limitation: they directly align the intermediate features between the teacher and student models. Some studies [Cho and Hariharan \(2019\)](#); [Mirzadeh et al. \(2020\)](#) have demonstrated that due to differences in model capacity and feature mapping methods, there are significant discrepancies between teacher and student features, including feature space distributions and semantic levels. Therefore, directly aligning such possibly mismatched features may even lead to negative optimization of the student model, thereby degrading its performance. To alleviate the discrepancy between teacher and student, many works resort to well-designed feature processing methods [Yang et al. \(2021\)](#); [Huang et al. \(2023\)](#) and loss functions [Ahn et al. \(2019\)](#); [Tian et al. \(2019a\)](#). Although these works improve the compatibility between teacher and student, the discrepancy is inherent and its optimization is still an intractable problem.

To address this issue, we hope to leverage the feature from the student itself as the supervision signals

for distillation. Therefore, we further propose teacher-guided student **Diffusion Self-KD**, dubbed as DSKD. DSKD introduces a teacher-classifier-guided diffusion model to denoise the student features, and the denoised features are regarded as the supervision target. Instead of directly aligning teacher and student features that previous works have done, DSKD performs distillation between the original and denoised student features. *The reasons why denoised student features could be seen as the distillation target are two aspects:* (1) The diffusion model is trained by teacher features to learn meaningful feature denoising capability, which is then used for student feature denoising. (2) Moreover, the denoising process of student features is also guided by the teacher classifier. Therefore, the teacher knowledge could be implicitly transferred to the denoised student features. By the way, the denoised student features naturally do not have discrepancies with the original student features.

It is worth mentioning that a previous seminal work called DiffKD [Huang et al. \(2023\)](#) also utilizes a diffusion model to denoise student features. Compared to DiffKD, our DSKD differs in three critical aspects: (1) **Diffusion model.** DiffKD uses a conventional diffusion model without extra optimization. By contrast, our DSKD adopts *teacher-classifier-guided* diffusion model for student feature sampling, emphasizing class-related information from the teacher network, which is beneficial to especially visual recognition tasks. (2) **Distillation supervision.** DiffKD still follows the traditional teacher-student alignment paradigm, leading to a potential discrepancy problem, as discussed above. Moreover, the denoised student features often have encoded teacher knowledge, therefore aligning the former with latter may *cancel out* those common information, leading to the information loss for the original student features. By contrast, our DSKD regards the denoised student features as the virtual teacher role to distill the original student features, avoiding the gap of feature distributions between teacher and student while learning the teacher’s knowledge effectively. (3) **Distillation loss.** Compared to the traditional Mean Squared Error (MSE) loss, we propose locality-sensitive hashing [Datar et al. \(2004\)](#) (LSH)-guided feature distillation that emphasizes more on feature direction than magnitude. We also provide theoretical proofs to justify the effectiveness of LSH.

We conduct image classification and semantic segmentation experiments to evaluate our method. Experimental results show that our DSKD achieves the best performance compared to recent state-of-the-art distillation methods on both homogeneous and heterogeneous architectures. Visualization results further demonstrate that the student learns similar feature patterns with the teacher even if we do not guide the student to mimic the teacher directly.

Our contributions are mainly divided into three aspects: (1) We introduce *teacher-classifier-guided* diffusion model to denoise the student features and augment them with class-related information. (2) We propose LSH-guided self-KD to avoid negative optimization towards teacher-student discrepancy, and force the student to focus on align feature direction. (3) DSKD achieves the best performance across classification and segmentation tasks.

2 Related Work

2.1 Knowledge Distillation

Knowledge Distillation (KD) aims to transfer meaningful knowledge from a powerful teacher to a weak student, therefore improving the student performance. The original KD [Hinton et al. \(2015\)](#) aligns the final class probability distributions between teacher and student, which is intuitive yet effective. This way ignores the intermediate feature information among the hidden layers. Therefore, many works explore feature-based distillation to provide more comprehensive guidance.

The seminal FitNet [Romero et al. \(2014\)](#) proposes to align teacher and student intermediate features in a layer-by-layer manner, making the student learn the feature extraction process from the teacher. However, this method does not consider higher-level feature modeling to explore more advanced feature knowledge forms. To address this issue, many works attempt to mine richer knowledge encoded in the original feature maps, such as attention maps [Zagoruyko and Komodakis \(2016\)](#); [Guo et al. \(2023\)](#); [Pham et al. \(2024\)](#), relationships [Park et al. \(2019\)](#); [Yang et al. \(2022b\)](#), contrastive representations [Tian et al. \(2019a\)](#); [Zhu et al. \(2021\)](#); [Yang et al. \(2023\)](#), multi-scale fusion [Chen et al. \(2021\)](#); [Wei et al. \(2024\)](#), and so on. Recently, DiffKD [Huang et al. \(2023\)](#) also introduces a diffusion model to assist the distillation process. Our DSKD outperforms DiffKD by

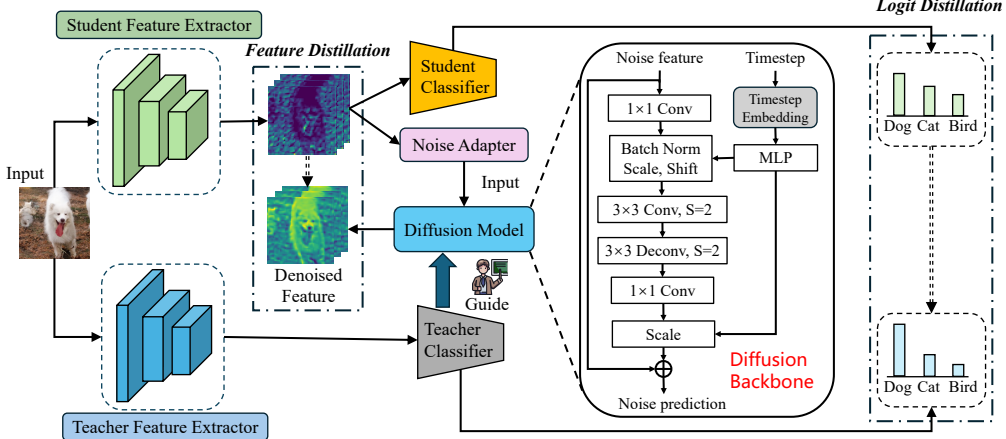


Figure 1 The overview of our proposed DSKD. We design a highly efficient yet effective diffusion backbone by combining the advantages of U-Net Ronneberger et al. (2015) and diffusion transformer (DiT) Peebles and Xie (2023). Inspired by DiT, we apply a Multi-Layer Perceptron (MLP) to regress scale and shift parameters for batch normalization layer, and scaling parameters before residual summation, from the conditioned timestep embedding. Inspired by U-Net, we first adopt a 3×3 convolution with stride $S = 2$ for downsampling and then a 3×3 deconvolution with stride $S = 2$ for upsampling. The final noise prediction is formulated as a residual output.

a more advanced *teacher-classifier-guided* diffusion model and a student-friendly self-distillation loss.

2.2 Diffusion Model

Denoising Diffusion Probabilistic Model (DDPM) Ho et al. (2020) has become a well-known generative paradigm for high-quality image generation. It often includes a forward and reverse process. During the forward process, the diffusion model progressively adds noise through multiple steps starting from a real image and obtains pure randomness like Gaussian noise. During the reverse process, the diffusion model learns to reverse this process by predicting and removing noise step-by-step, reconstructing the original image from randomness. Song et al. Song et al. (2020) proposed Denoising Diffusion Implicit Model (DDIM) that constructs non-Markovian diffusion processes to obtain deterministic generation, leading to faster generation. Dhariwal et al. Dhariwal and Nichol (2021) proposed to improve diffusion models with classifier guidance for a better trade-off between diversity and fidelity using gradients from an extra classifier. More detailed discussions could refer to Croitoru et al.'s survey Croitoru et al. (2023).

Recently, some distillation works Salimans and Ho (2022); Sun et al. (2023); Feng et al. (2024) are proposed to accelerate the diffusion model by reducing the number of iterative steps. Their core idea is to regard the original diffusion model with complete steps as the teacher, and the counterpart with reduced steps as the student. The distillation loss guides the student to match the teacher's denoised trajectory. Therefore, the distilled student could generate high-quality images using only very few steps. **Beyond distilling diffusion model itself, using diffusion model to improve visual recognition distillation is also a promising direction but highly ignored.**

3 Methodology

We introduce teacher-classifier-guided diffusion model to denoise the student features. In this way, the teacher model's knowledge can be implicitly transferred to the student features. We then align the original student features to the denoised student features. This allows the student model to learn from the teacher without considering the negative discrepancy. The overview of DSKD is shown in Figure 1.

3.1 Preliminary: Diffusion Model

Forward noising process. Given a sample $\mathbf{x}_0 \sim q(\mathbf{x}_0)$ from the data distribution, the forward process progressively adds Gaussian noise for T diffusion steps according to the noise schedule β_1, \dots, β_T :

$$q(\mathbf{x}_t | \mathbf{x}_{t-1}) = \mathcal{N}(\mathbf{x}_t; \sqrt{1 - \beta_t} \mathbf{x}_{t-1}, \beta_t \mathbf{I}). \quad (1)$$

Finally, $\mathbf{x}_T \sim \mathcal{N}(\mathbf{0}, \mathbf{I})$ is pure Gaussian noise. A noisy sample \mathbf{x}^t could be formulated as a one-step equation:

$$q(\mathbf{x}_t | \mathbf{x}_0) = \mathcal{N}(\mathbf{x}_t; \sqrt{\bar{\alpha}_t} \mathbf{x}_0, (1 - \bar{\alpha}_t) \mathbf{I}). \quad (2)$$

\mathbf{x}_t can be regarded as a linear combination of \mathbf{x}_0 and noise variable ϵ_t :

$$\mathbf{x}_t = \sqrt{\bar{\alpha}_t} \mathbf{x}_0 + \sqrt{1 - \bar{\alpha}_t} \epsilon_t, \quad (3)$$

where $\alpha_t := 1 - \beta_t$, $\bar{\alpha}_t := \prod_{s=0}^t \alpha_s$ and $\epsilon_t \sim \mathcal{N}(\mathbf{0}, \mathbf{I})$.

Optimization. During the training phase, a noise predictor ϵ_θ is optimized to predict the noise in \mathbf{x}_t by minimizing the MSE loss between \mathbf{x}_t and the original image \mathbf{x}_0 :

$$\mathcal{L}_{\text{Diff}} = \mathbb{E}_{\mathbf{x}_0, \epsilon_t, t} [\|\epsilon_t - \epsilon_\theta(\mathbf{x}_t, t)\|^2]. \quad (4)$$

Reverse process. During the test phase, \mathbf{x}_0 is reconstructed by starting from Gaussian noise $\mathbf{x}_T \sim \mathcal{N}(\mathbf{0}, \mathbf{I})$ and iteratively denoising with the trained noise predictor ϵ_θ :

$$p_\theta(\mathbf{x}_{t-1} | \mathbf{x}_t) := \mathcal{N}(\mathbf{x}_{t-1}; \epsilon_\theta(\mathbf{x}_t, t), \sigma_t^2 \mathbf{I}), \quad (5)$$

where σ_t is a transition variance in DDIM. Different σ_t values would lead to distinct generative processes. When $\sigma_t = \sqrt{(1 - \alpha_{t-1}) / (1 - \alpha_t)} \sqrt{1 - \alpha_t / \alpha_{t-1}}$ for all t , the forward process becomes Markov chain, and the reverse process is equivalent to DDPM.

3.2 Teacher-Guided Student Feature Denoising

Inspired by the work *classifier-guided diffusion model* Dhariwal and Nichol (2021), we designed a new feature distillation method by using the teacher model to guide the reverse denoising process of the student features. Under the teacher’s guidance, the distribution of the student features shifts towards that of the teacher features, enriching the student features with meaningful semantic information from the teacher.

The denoising process of classifier-guided diffusion model Dhariwal and Nichol (2021) is formulated as:

$$p_{\theta, \phi}(\mathbf{x}_t | \mathbf{x}_{t+1}, y) = Z p_\theta(\mathbf{x}_t | \mathbf{x}_{t+1}) p_\phi(y | \mathbf{x}_t). \quad (6)$$

Here, the definition of each variable follows the original paper Dhariwal and Nichol (2021). Z is a normalizing constant, $p_\theta(\mathbf{x}_t | \mathbf{x}_{t+1})$ is an unconditional reverse noising process following DDPM Ho et al. (2020), and $p_\phi(y | \mathbf{x}_t)$ is a classifier, where \mathbf{x}_t is the noise image at the t -th step, and y is a class label.

In the context of teacher-student distillation, we formulate $p_\phi(y | \mathbf{x}_t)$ as the pre-trained teacher classifier, and \mathbf{x}_t as the denoised student features at the t -th step. Unlike the traditional denoising formula, we condition the sampling process on the student features $\mathbf{f}^{(stu)} \in \mathbb{R}^{H \times W \times D}$, where H , W , and C represent height, width, and the number of channels, respectively. We start $\mathbf{f}^{(stu)}$ as \mathbf{x}_T to perform teacher-guided diffusion sampling by T steps, i.e. $t = T, \dots, 2, 1$. \mathbf{x}_t denotes the denoised student features at the t -th time step. Therefore, the sampling formula of Equ.(17) can be expressed as follows:

$$p(\mathbf{x}_t | \mathbf{x}_{t+1}, y; \theta, \phi^{(tea)}) = Z p_\theta(\mathbf{x}_t | \mathbf{x}_{t+1}) p(y | \mathbf{x}_t; \phi^{(tea)}). \quad (7)$$

$p(\mathbf{x}_t | \mathbf{x}_{t+1}, y; \theta, \phi^{(tea)})$ is a conditional Markov process to denoise the student feature from \mathbf{x}_{t+1} to \mathbf{x}_t , conditioned by the noise predictor θ and the teacher classifier $\phi^{(tea)}$. $p(y | \mathbf{x}_t; \phi^{(tea)})$ is the conditional probability of the predicted class y based on the student features \mathbf{x}_t inferred from the teacher classifier $\phi^{(tea)}$. The teacher classifier often includes a global average pooling layer and a linear weight matrix to output

class probability distribution. We adopt the traditional diffusion model that predicts \mathbf{x}_t from \mathbf{x}_{t+1} according to a Gaussian distribution:

$$p_{\theta}(\mathbf{x}_t | \mathbf{x}_{t+1}) = \mathcal{N}(\boldsymbol{\mu}, \boldsymbol{\Sigma}), \quad (8)$$

where $\boldsymbol{\mu} = \boldsymbol{\mu}_{\theta}(\mathbf{x}_{t+1})$, $\boldsymbol{\Sigma} = \boldsymbol{\Sigma}_{\theta}(\mathbf{x}_{t+1})$. The logarithm form of Equ.(19) is formulated as:

$$\log p_{\theta}(\mathbf{x}_t | \mathbf{x}_{t+1}) = -\frac{1}{2}(\mathbf{x}_t - \boldsymbol{\mu})^\top \boldsymbol{\Sigma}^{-1}(\mathbf{x}_t - \boldsymbol{\mu}) + C. \quad (9)$$

When the number of diffusion steps is limited to be infinite, we can derive $\|\boldsymbol{\Sigma}\| \rightarrow \mathbf{0}$. In this case, $p(y|\mathbf{x}_t; \boldsymbol{\phi}^{(tea)})$ has low curvature compared to $\boldsymbol{\Sigma}^{-1}$. Therefore, we can approximate $\log p(y|\mathbf{x}_t; \boldsymbol{\phi}^{(tea)})$ by a first-order Taylor expansion at $\mathbf{x}_t = \boldsymbol{\mu}$:

$$\begin{aligned} \log p(y|\mathbf{x}_t; \boldsymbol{\phi}^{(tea)}) &\approx \log p(y|\mathbf{x}_t; \boldsymbol{\phi}^{(tea)})|_{\mathbf{x}_t=\boldsymbol{\mu}} \\ &+ (\mathbf{x}_t - \boldsymbol{\mu}) \nabla_{\mathbf{x}_t} \log p(y|\mathbf{x}_t; \boldsymbol{\phi}^{(tea)})|_{\mathbf{x}_t=\boldsymbol{\mu}} \\ &= (\mathbf{x}_t - \boldsymbol{\mu}) \mathbf{g} + C_1, \end{aligned} \quad (10)$$

where $\mathbf{g} = \nabla_{\mathbf{x}_t} \log p(y|\mathbf{x}_t; \boldsymbol{\phi}^{(tea)})|_{\mathbf{x}_t=\boldsymbol{\mu}}$, and C_1 can be regarded as a constant. We can further derive the logarithm form of Equ.(18) as:

$$\log(p_{\theta}(\mathbf{x}_t | \mathbf{x}_{t+1}) p(y|\mathbf{x}_t; \boldsymbol{\phi}^{(tea)})) \approx \log p(\mathbf{z}), \quad (11)$$

where $\mathbf{z} \sim \mathcal{N}(\boldsymbol{\mu} + \boldsymbol{\Sigma} \mathbf{g}, \boldsymbol{\Sigma})$. The detailed proof is shown in Appendix A.1. Therefore, the conditional sampling strategy can be approximated to the unconditional Gaussian sampling, but differs in the shifted mean by $\boldsymbol{\Sigma} \mathbf{g}$. Moreover, we introduce a gradient scale k as the guidance strength over the gradient of the teacher classifier. In summary, the teacher-guided diffusion sampling is formulated as:

$$\mathbf{x}_{t-1} \sim \mathcal{N}(\boldsymbol{\mu} + k \boldsymbol{\Sigma} \nabla_{\mathbf{x}_t} \log p(y|\mathbf{x}_t; \boldsymbol{\phi}^{(tea)}), \boldsymbol{\Sigma}). \quad (12)$$

In theory, the gradient scale k can smooth the teacher class probability distribution, proportional to $p(y|\mathbf{x}_t; \boldsymbol{\phi}^{(tea)})^k$. When $k > 1$, the distribution becomes sharper, meaning that the teacher classifier has stronger guidance strength, resulting in higher fidelity (but less diverse) image features.

After the teacher-guided diffusion sampling process proceeds by T steps, the original student features $\mathbf{f}^{(stu)}$ (*i.e.* \mathbf{x}_T) is converted to the denoised student features $\hat{\mathbf{f}}^{(stu)}$ (*i.e.* \mathbf{x}_0). According to Table 8, we set $T = 2$ and $T = 3$ on CIFAR-100 and ImageNet, respectively.

3.3 LSH-Guided Student Self-Feature Distillation

Our method uses classifier-guided diffusion model as the generator for sampling student features, making the distribution of denoised student feature $\hat{\mathbf{f}}^{(stu)}$ more similar to that of the teacher feature $\boldsymbol{\phi}^{(tea)}$. This lets the denoised student feature $\hat{\mathbf{f}}^{(stu)}$ learn similar semantic information and representation capability from the teacher feature $\boldsymbol{\phi}^{(tea)}$ implicitly. Moreover, since the teacher model often has powerful discriminative capability, the denoised student feature $\hat{\mathbf{f}}^{(stu)}$ could preserve class-related information during the teacher-guided diffusion sampling process compared to the conventional teacher-agnostic DiffKD [Huang et al. \(2023\)](#).

In the context of the distillation process, student features are considered to be the “noisy version” of teacher model features, as demonstrated by DiffKD [Huang et al. \(2023\)](#). We also introduce a *noise adapter* to initialize the noise level of student features, whose details are shown in Appendix A.2. After the teacher-guided student feature diffusion sampling process, the original student feature $\mathbf{f}^{(stu)}$ would be transformed to the teacher-guided denoised student feature $\hat{\mathbf{f}}^{(stu)}$.

Unlike most previous KD methods including DiffKD that use the teacher to distill the student, our DSKD method utilizes the denoised student feature $\hat{\mathbf{f}}^{(stu)}$ to distill the original student feature $\mathbf{f}^{(stu)}$ via comprehensive local and global distillation. The local distillation follows a traditional paradigm by aligning the full feature-maps via a simple MSE loss:

$$\mathcal{L}_{\text{Local}} = \left\| \mathbf{f}^{(stu)} - \hat{\mathbf{f}}^{(stu)} \right\|_2^2, \quad (13)$$

Algorithm 1 Teacher-guided student self-knowledge distillation using diffusion model

Input: diffusion model $(\mu_\theta(\mathbf{x}_t), \Sigma_\theta(\mathbf{x}_t))$, pretrained teacher feature extractor $\Phi^{(tea)}$ and classifier $\phi^{(tea)}$, untrained student feature extractor $\Phi^{(stu)}$, dataset \mathcal{D} .

Output: the trained student model.

```

1: for each  $(\mathbf{x}, y) \in \mathcal{D}$  do
2:   Extract features:  $\mathbf{f}^{(tea)} = \Phi^{(tea)}(\mathbf{x})$ ,  $\mathbf{f}^{(stu)} = \Phi^{(stu)}(\mathbf{x})$ 
3:   Train the diffusion model  $(\mu_\theta(\mathbf{x}_t), \Sigma_\theta(\mathbf{x}_t))$  using  $\mathbf{f}^{(tea)}$  by  $\mathcal{L}_{\text{Diff}}$  (Equ.(4)).
4:   Start at  $\mathbf{f}^{(stu)}$  as  $\mathbf{x}_T$  to perform teacher-guided diffusion denoising sampling.
5:   for all  $t$  from  $T$  to 1 do
6:      $\mu, \Sigma \leftarrow \mu_\theta(\mathbf{x}_t), \Sigma_\theta(\mathbf{x}_t)$ 
7:      $\mathbf{x}_{t-1} \sim \mathcal{N}(\mu + k\Sigma \nabla_{\mathbf{x}_t} \log p(y|\mathbf{x}_t; \phi^{(tea)}), \Sigma)$ 
8:   end for
9:   Compute the DSKD loss  $\mathcal{L}_{\text{DSKD}}$  (Equ.(15)) between the original and denoised student features of
 $\mathbf{f}^{(stu)}$  and  $\hat{\mathbf{f}}^{(stu)}$  (i.e.  $\mathbf{x}_0$ ).
10:  Compute the basic task loss  $\mathcal{L}_{\text{Task}}$  by cross-entropy.
11:  Compute the Hinton's distillation loss  $\mathcal{L}_{\text{KD}}$ .
12:  Update the student model by optimizing  $\mathcal{L}_{\text{Train}}$ .
13: end for
14:

```

which makes the student learn spatially dense semantic information. On the other hand, we further apply global average pooling to $\mathbf{f}^{(stu)}$ and $\hat{\mathbf{f}}^{(stu)}$, and output $\mathbf{v}^{(stu)} \in \mathbb{R}^D$ and $\hat{\mathbf{v}}^{(stu)} \in \mathbb{R}^D$ as global feature embeddings, respectively. Unlike local features that may contain noisy information, the global features encode robust object-centric representations. And then we construct a novel locality-sensitive hashing [Datar et al. \(2004\)](#) (LSH) Guided global distillation method for aligning $\mathbf{v}^{(stu)}$ and $\hat{\mathbf{v}}^{(stu)}$. In this approach, we adopt M hash functions, and construct M binary codes for denoised student feature $\hat{\mathbf{v}}^{(stu)}$. The hash code of original student feature $\mathbf{v}^{(stu)}$ is required to be identical to that of denoised student feature $\hat{\mathbf{v}}^{(stu)}$. Therefore, we formulate this problem as minimizing a binary cross-entropy classification loss:

$$\mathcal{L}_{\text{Global}} = -\frac{1}{M} \sum_{m=1}^M [\delta_m \log \rho_m + (1 - \delta_m) \log(1 - \rho_m)], \quad (14)$$

where $\boldsymbol{\delta} = \text{sign}(\mathbf{W}^\top \hat{\mathbf{v}}^{(stu)} + \mathbf{b}) \in \mathbb{R}^M$, $\boldsymbol{\rho} = \text{Sigmoid}(\mathbf{W}^\top \mathbf{v}^{(stu)} + \mathbf{b}) \in \mathbb{R}^M$, $\mathbf{W} \in \mathbb{R}^{D \times M}$ represents projection matrix whose values are sampled from a Gaussian distribution, and $\mathbf{b} \in \mathbb{R}^M$ denotes the bias. We set $M = 256$ according to [Appendix 4.7](#). Inspired by FNKD [Xu et al. \(2020\)](#), feature direction is more important than its magnitude. LSH can also achieve this goal that relaxes the constraints of feature distillation on magnitude, but prioritize feature direction alignment.

The overall loss of DSKD is formulated as the summation of $\mathcal{L}_{\text{Local}}$ and $\mathcal{L}_{\text{Global}}$:

$$\mathcal{L}_{\text{DSKD}} = \mathcal{L}_{\text{Local}} + \gamma \mathcal{L}_{\text{Global}}, \quad (15)$$

where γ is a loss weight and we found $\gamma = 1$ works well. In this way, DSKD can guide the student to learn meaningful knowledge from the more powerful teacher indirectly through a diffusion model. Notice that the conventional KD methods often have the representational gap problem between teacher and student, and they often resort to complex training schemes, loss functions, and feature alignment techniques to alleviate this issue. By contrast, our DSKD eliminates the inherent difference of teacher-student feature distributions and guides the student to learn compatible information with the teacher.

3.4 Overall Training Process

The overview of the proposed DSKD is shown in [Algorithm 1](#). First, we extract teacher and student features $\mathbf{f}^{(tea)}$ and $\mathbf{f}^{(stu)}$. We regard $\mathbf{f}^{(tea)}$ as \mathbf{x}_0 in the forward noise process $q(\mathbf{x}_t|\mathbf{x}_0)$ (Equ.(2)) and then train the teacher-guided diffusion model by $\mathcal{L}_{\text{Diff}}$ (Equ.(4)). We start at $\mathbf{f}^{(stu)}$ as \mathbf{x}_T to perform teacher-guided diffusion denoising sampling by Equ.(23) with T time steps. After the denoising process, the denoised student

Table 1 Training strategies on image classification tasks. **BS**: batch size; **LR**: learning rate; **WD**: weight decay.

Strategy	Dataset	Epochs	Total BS	Initial LR	Optimizer	WD	LR scheduler	Data augmentation
A1	CIFAR-100	240	64	0.05	SGD	5×10^{-4}	$\times 0.1$ at 150,180,210 epochs	crop + flip
B1	ImageNet	100	256	0.1	SGD	1×10^{-4}	$\times 0.1$ every 30 epochs	crop + flip
B2	ImageNet	300	1024	0.001	AdamW	0.05	cosine decay	Liu et al. (2021)

Table 2 Top-1 accuracy of different distillation methods under homogeneous and heterogeneous architecture styles on CIFAR-100 dataset. We follow the training strategy A1 in Table 1.

Method	Homogeneous architecture style			Heterogeneous architecture style		
	WRN-40-2	ResNet-56	ResNet-32x4	ResNet-56	WRN-40-2	ResNet-32x4
	WRN-40-1	ResNet-20	ResNet-8x4	WRN-40-1	ResNet-20	ResNet-20
Teacher	75.61	72.34	79.42	72.34	75.61	79.42
Student	71.98	69.06	72.50	71.98	69.06	69.06
KD Hinton et al. (2015)	73.54 ± 0.20	70.66 ± 0.24	73.33 ± 0.20	73.39 ± 0.17	71.15 ± 0.22	70.21 ± 0.09
FitNet Romero et al. (2014)	72.24 ± 0.24	69.21 ± 0.36	73.50 ± 0.28	72.22 ± 0.28	69.34 ± 0.20	69.81 ± 0.07
VID Ahn et al. (2019)	73.30 ± 0.13	70.38 ± 0.14	73.09 ± 0.21	73.37 ± 0.16	70.41 ± 0.18	70.35 ± 0.11
RKD Park et al. (2019)	72.22 ± 0.20	69.61 ± 0.06	71.90 ± 0.11	72.16 ± 0.23	69.59 ± 0.18	69.76 ± 0.18
PKT Passalis et al. (2020)	73.45 ± 0.19	70.34 ± 0.20	73.64 ± 0.18	73.23 ± 0.19	69.92 ± 0.13	70.28 ± 0.20
CRD Tian et al. (2019a)	74.14 ± 0.22	71.16 ± 0.17	75.51 ± 0.18	74.06 ± 0.20	71.03 ± 0.19	71.19 ± 0.14
CTKD Li et al. (2023)	73.93 ± 0.17	71.19 ± 0.28	76.44 ± 0.32	73.68 ± 0.15	71.24 ± 0.26	71.18 ± 0.33
DiffKD Huang et al. (2023)	74.09 ± 0.09	71.92 ± 0.14	76.72 ± 0.15	73.99 ± 0.13	71.60 ± 0.27	71.39 ± 0.21
CAT-KD Guo et al. (2023)	74.26 ± 0.07	71.64 ± 0.15	76.88 ± 0.09	73.68 ± 0.21	71.58 ± 0.13	71.21 ± 0.06
LS Sun et al. (2024)	74.33 ± 0.08	71.43 ± 0.16	76.59 ± 0.11	73.71 ± 0.24	71.47 ± 0.28	71.27 ± 0.33
SD Wei et al. (2024)	73.86 ± 0.13	71.35 ± 0.27	76.53 ± 0.18	73.83 ± 0.34	71.42 ± 0.14	71.30 ± 0.20
IKD Wang et al. (2025)	74.16 ± 0.11	71.83 ± 0.23	76.58 ± 0.17	73.47 ± 0.35	71.28 ± 0.29	70.89 ± 0.14
DSKD (Ours)	74.45 ± 0.16	72.26 ± 0.12	77.08 ± 0.10	74.70 ± 0.07	72.13 ± 0.19	71.63 ± 0.14

feature $\hat{\mathbf{f}}^{(stu)}$ is produced. We compute the DSKD loss (Equ.(13)) between the original and denoised student features of $\mathbf{f}^{(stu)}$ and $\hat{\mathbf{f}}^{(stu)}$. Moreover, the task loss $\mathcal{L}_{\text{Task}}$ is the conventional cross-entropy loss between the student class probability and ground-truth label. The \mathcal{L}_{KD} loss is KL-divergence between teacher and student class probability distributions following by [Hinton et al. Hinton et al. \(2015\)](#). In summary, the overall loss is formulated as:

$$\mathcal{L}_{\text{Train}} = \mathcal{L}_{\text{Task}} + \alpha \mathcal{L}_{\text{DSKD}} + \mathcal{L}_{\text{Diff}} + \mathcal{L}_{\text{KD}}, \quad (16)$$

where α is the DSKD loss weight, and we set $\alpha = 1$ according to Figure 3. We do not introduce extra weights for the basic $\mathcal{L}_{\text{Task}}$, $\mathcal{L}_{\text{Diff}}$, and \mathcal{L}_{KD} following previous works [Yang et al. \(2021, 2022b\); Huang et al. \(2023\)](#).

4 Experiments

4.1 Experimental Setup

Datasets. We adopt CIFAR-100 [Krizhevsky and Hinton \(2009\)](#) and ImageNet [Deng et al. \(2009\)](#) datasets for image classification. CIFAR-100 dataset consists of 50K training images and 10K testing images across 100 classes. ImageNet is a large-scale dataset composed of 1.2 million training images and 50K validation images in 1000 classes. ADE20K [Zhou et al. \(2017\)](#) contains 20K training images and 2K validation images with 150 semantic categories under diverse scenes for large-scale semantic segmentation.

Network architecture. We use famous network families for evaluation, including ResNet [He et al. \(2016\)](#), WRN [Zagoruyko S \(2016\)](#), MobileNetV1 [Howard et al. \(2017\)](#), MobileNetV3 [Howard et al. \(2019\)](#), Swin Transformer [Liu et al. \(2021\)](#), and DeepLabV3 [Chen et al. \(2018\)](#).

Table 3 Accuracy results on ImageNet following the training strategy B1 in Table 1.

Teacher	Student	Metric	Tea.	Stu.	KD	Review	DKD	CTKD	DiffKD	CAT-KD	LS	SD	IKD	RLD	DSKD
ResNet-34	ResNet-18	Top-1	73.31	69.76	70.66	71.61	71.70	71.32	72.22	71.26	71.42	71.44	71.82	71.91	72.57
		Top-5	91.42	89.08	89.88	90.51	90.41	90.27	90.64	90.45	90.29	90.05	90.57	90.59	90.82
ResNet-50	MobileNetV1	Top-1	76.16	70.13	70.68	72.56	72.05	72.87	73.27	72.24	72.18	72.24	73.27	72.75	73.73
		Top-5	92.86	89.49	90.30	91.00	91.05	91.29	91.14	91.13	90.80	90.71	91.34	91.18	91.52

Table 4 Top-1 accuracy results of ResNet-18 on ImageNet compared with recent self-distillation methods.

Method	Stu.	BYOT	Tf-KD	CS-KD	PS-KD	FRSKD	DLB	MixSKD	FASD	DSKD
Acc	69.76	71.34	70.44	70.65	70.96	71.36	70.93	71.52	71.43	72.57

Compared methods We compare our method with recent representative teacher-student distillation methods, including KD Hinton et al. (2015), Review Chen et al. (2021), DKD Zhao et al. (2022), Manifold Hao et al. (2022), CTKD Li et al. (2023), DiffKD Huang et al. (2023), CAT-KD Guo et al. (2023), LS Sun et al. (2024), SD Wei et al. (2024), IKD Wang et al. (2025), and RLD Sun et al. (2025). Moreover, we also include self-distillation methods, including BYOT Zhang et al. (2019), Tf-KD Yuan et al. (2020), CS-KD Yun et al. (2020), PS-KD Kim et al. (2021), FRSKD Ji et al. (2021), DLB Shen et al. (2022), MixSKD Yang et al. (2022a), FASD Xu et al. (2024).

4.2 Experimental Results on Image Classification

Table 2 shows the compared results on CIFAR-100. Compared with state-of-the-art IKD, our DSKD achieves 0.40% and 0.94% average improvements on homogeneous and heterogeneous architecture pairs, respectively. As shown in Table 3, DSKD also performs the best on the large-scale ImageNet dataset. DSKD outperforms IKD on ResNet-18 and MobileNetV1 by 0.75% and 0.46% top-1 accuracy gains, respectively. Table 5 exhibits the ImageNet results on Swin Transformer. DSKD obtains the highest 82.8% accuracy on Swin-Tiny, surpassing DiffKD and IKD by 0.4% and 0.8%, respectively. The results verify that our DSKD could well adapt to vision Transformer architecture. Overall results demonstrate that teacher-guided diffusion denoising is an effective way to student feature self-distillation.

4.3 Results on Semantic Segmentation

Table 6 shows the extended results for semantic segmentation on ADE20K, where the training settings are followed by CIRKD Yang et al. (2022b). DSKD also achieves the best performance and exceeds state-of-the-art DiffKD and LAD by 1.73% and 1.97% mIoU improvements, respectively. The results demonstrate that DSKD can be well transferred to the downstream semantic segmentation task.

4.4 Comparison with Self-Distillation methods

Although our DSKD is a teacher-student-based distillation method, we also compare those teacher-free self-distillation methods in Table 4. DSKD achieves the best performance and outperforms SOTA MixSKD by 1.05%. A weakness of teacher-free self-distillation is the limited performance upper bound due to the lack of a teacher. By contrast, our DSKD constructs target features denoised by a teacher-guided diffusion model, making the student learn from the teacher.

4.5 Ablation Study and Analysis

By default, the experimental teacher-student pair is WRN-40-2&WRN-40-1 for CIFAR-100 and ResNet-34&ResNet-18 for ImageNet.

Analysis of guidance strengths. The guidance strength refers to the hyper-parameter k to reweight the gradient of the teacher classifier $\nabla_{\mathbf{x}_t} \log p(y|\mathbf{x}_t; \phi^{(tea)})$ during the diffusion denoising process. When $k > 1$, the

Table 5 Top-1 accuracy results of Swin Transformer on ImageNet following the training strategy B2 in Table 1.

Teacher	Student	Tea.	Stu.	KD	Manifold	DiffKD	IKD	DSKD
Swin-Base	Swin-Tiny	83.5	81.3	81.8	82.3	82.4	82.0	82.8

Table 6 Performance comparison with semantic segmentation distillation methods on ADE20K.

Method	mIoU (%)
T: DeepLabV3-ResNet-101	43.83
S: DeepLabV3-MobileNetV3-Large	32.83
+SKD Liu et al. (2019)	33.78
+IFVD Wang et al. (2020)	34.21
+CWD Shu et al. (2021)	34.18
+DSD Feng et al. (2021)	33.64
+CIRKD Yang et al. (2022b)	35.15
+APD Tian et al. (2022)	34.53
+Af-DCD Fan et al. (2023)	35.12
+DiffKD Huang et al. (2023)	34.85
+LAD Liu et al. (2024)	34.61
+DSKD (Ours)	36.58

distribution becomes sharper, resulting in higher fidelity (but less diverse) image features. As shown in Figure 2, we investigated the effects of different guidance strengths on CIFAR-100 and ImageNet datasets. We found that $k = 1$ and $k = 2$ achieve the best performance on CIFAR-100 and ImageNet, respectively. Lower k may weaken the strength of teacher guidance, while higher k would decrease the diversity of image features. Moreover, we found that ImageNet needs a larger k than CIFAR-100, because ImageNet is a more diverse and higher resolution image dataset than CIFAR-100.

Effect of DSKD Loss. To evaluate the impact of the proposed DSKD loss term ($\mathcal{L}_{\text{Local}}$ and $\mathcal{L}_{\text{Global}}$), we conducted an ablation study on ImageNet in Table 7. When only the KD loss (\mathcal{L}_{KD}) is applied, the student model achieves an accuracy of 70.66%, which serves as the distillation baseline for comparison. By replacing \mathcal{L}_{KD} with DSKD-based $\mathcal{L}_{\text{Local}}$ and $\mathcal{L}_{\text{Global}}$, the accuracy increases to 72.17%, demonstrating that the DSKD loss is more effective than the traditional KD loss. Moreover, $\mathcal{L}_{\text{Global}}$ outperforms $\mathcal{L}_{\text{Local}}$ by 0.52%, indicating that LSH-guided global distillation is more important. Finally, when all losses of \mathcal{L}_{KD} , $\mathcal{L}_{\text{DSKD}}$, and $\mathcal{L}_{\text{Diff}}$ are combined, the accuracy is further boosted to 72.57%. This demonstrates the effectiveness of using denoised student features as the distillation supervision.

Table 7 Ablation study of distillation loss terms over ResNet-18 supervised by ResNet-34 on ImageNet.

Loss	Different loss combinations					
	\checkmark	\checkmark	\checkmark	\checkmark	\checkmark	\checkmark
$\mathcal{L}_{\text{Task}}$	\checkmark	\checkmark	\checkmark	\checkmark	\checkmark	\checkmark
$\mathcal{L}_{\text{Local}}$	-	\checkmark	-	\checkmark	-	\checkmark
$\mathcal{L}_{\text{Global}}$	-	-	\checkmark	\checkmark	-	\checkmark
$\mathcal{L}_{\text{Diff}}$	-	\checkmark	\checkmark	\checkmark	-	\checkmark
\mathcal{L}_{KD}	-	-	-	-	\checkmark	\checkmark
Accuracy	69.76	71.33	71.85	72.17	70.66	72.57

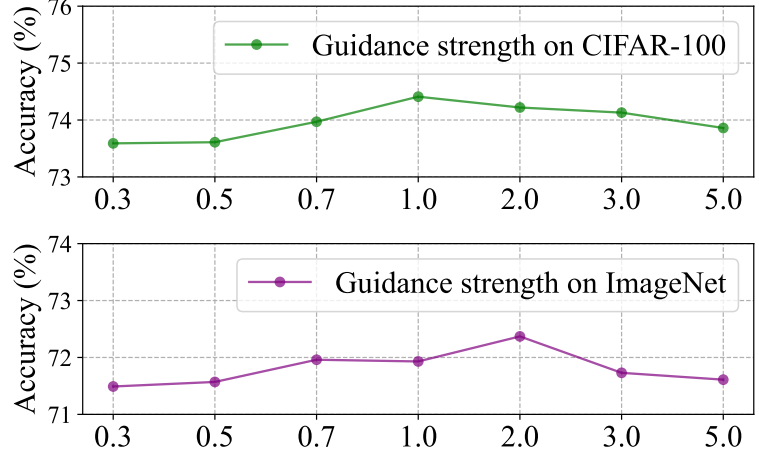


Figure 2 Analysis of various guidance strengths on CIFAR-100 and ImageNet datasets.

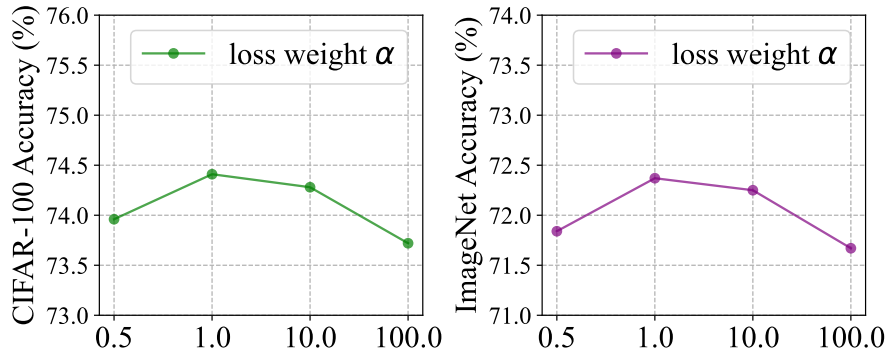


Figure 3 Analysis of the weight α of DSKD loss $\mathcal{L}_{\text{DSKD}}$ on CIFAR-100 and ImageNet datasets.

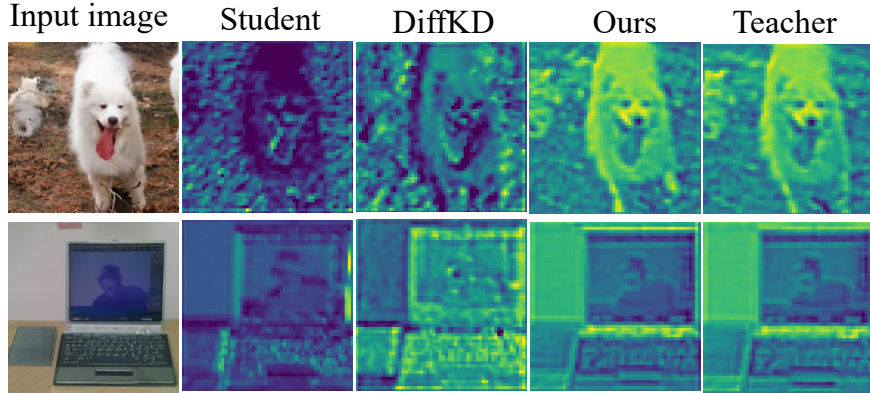


Figure 4 Visualizations of the original student features, DiffKD's denoised student features, our denoised student features, and teacher features on ImageNet.

Analysis of the weight α of DSKD loss. As shown in Figure 3, we examine the sensitivity of the loss weight α within $[0.5, 100]$. We found that $\alpha \in [1, 10]$ achieves good performance, and $\alpha = 1$ performs the best on both CIFAR-100 and ImageNet.

Visualization of denoised features. As shown in Figure 4, we visualize the original student features, denoised student features by DiffKD and our DSKD, teacher features during the distillation process. Compared to the original and DiffKD student features, we found that our denoised student features have more similar semantics and salient distributions with the teacher features. The results reveal that our method can remove noise

information over the original features effectively. Our teacher-classifier-guided diffusion process emphasizes more class-related semantics than DiffKD, therefore leading to better feature quality.

4.6 Analysis of The Number of Denoising Timesteps T

The number of denoising timesteps is an important factor for the denoising quality of student features. In Table 8, we investigate the impact on various numbers of denoising timesteps on CIFAR-100 and ImageNet. We observed that more timesteps generally produce better accuracy due to stronger denoising capability. However, more timesteps often generate additional training costs. And we found that $T = 2$ on CIFAR-100 and $T = 3$ on ImageNet are good enough for DSKD for pursuing the best efficiency-accuracy trade-off. We adopt the larger number of timesteps on ImageNet than that of timesteps on CIFAR-100, because the ImageNet’s images have larger resolution sizes and more complex objects than CIFAR-100’s images.

Table 8 Top-1 accuracy results under various numbers of denoising timesteps on CIFAR-100 and ImageNet.

Timesteps T	1	2	3	4	5
CIFAR-100	74.20	74.45	74.42	74.49	74.47
ImageNet	71.93	72.34	72.57	72.58	72.60

4.7 Analysis of the Number of Hash Functions M for LSH-Guided Feature Distillation

As shown in Table 9, we explore the number of hash functions M for LSH-guided feature distillation. In theory, a larger M reduces randomness of LSH for feature distillation. We observe that $M = 256$ achieves the best performance.

Table 9 Top-1 accuracy results under various numbers of hash functions M on CIFAR-100 and ImageNet.

Hash function number M	32	64	128	256	512
CIFAR-100	74.28	74.36	74.39	74.45	74.44
ImageNet	72.38	72.49	72.51	72.57	72.55

4.8 Analysis of Various Feature Distillation Mechanisms

We compare LSH-guided feature distillation mechanism with existing alternative feature distillation works like the traditional FitNet [Romero et al. \(2014\)](#) and FNKD [Xu et al. \(2020\)](#). As shown in Table 10, our LSE-guided feature distillation outperforms the existing popular feature distillation mechanisms.

Table 10 Top-1 accuracy results under various feature distillation mechanisms on CIFAR-100 and ImageNet.

Mechanisms	FitNet	FNKD	LSH
CIFAR-100	73.94	74.08	74.45
ImageNet	72.16	72.28	72.57

4.9 Analysis of Class Probability Distribution

As shown in Figure 5, we show the distributions of predicted class probabilities by ResNet-18 pretrained on ImageNet using teacher model, our DSKD, DiffKD, and the baseline student, respectively. Compared to DiffKD and baseline student, our DSKD leads to higher prediction quality: (1) Even in the case of an easy sample that all methods are correctly predicted, our DSKD assigns the highest probability to the correct class; (2) In the hard case, only DSKD makes correct predictions, while other methods produce error predictions. The results verify that our DSKD can guide the model to learn more similar distributions with the teacher.

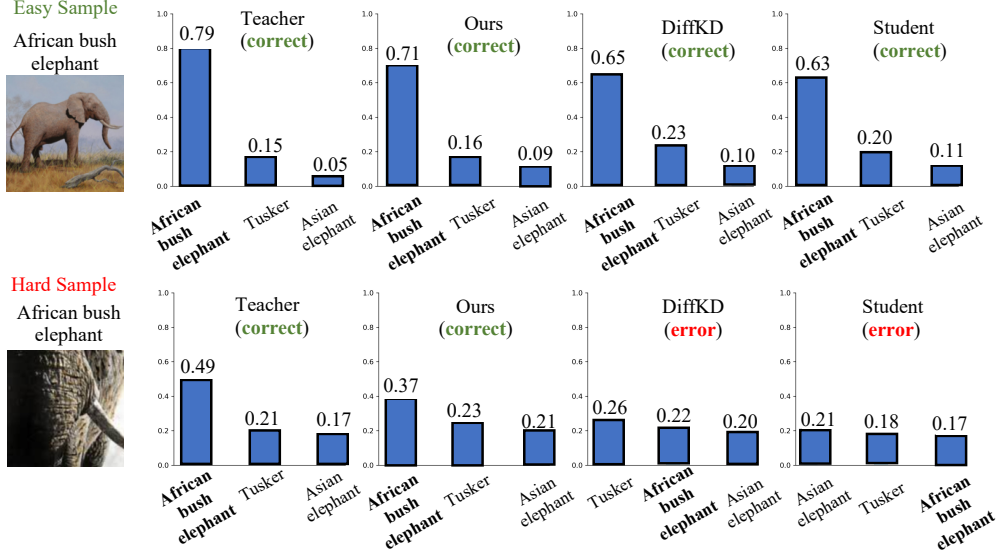


Figure 5 Illustrations of class probability distributions generated by ResNet-18 pretrained on ImageNet using teacher, our DSKD, DiffKD, and the baseline student, respectively.

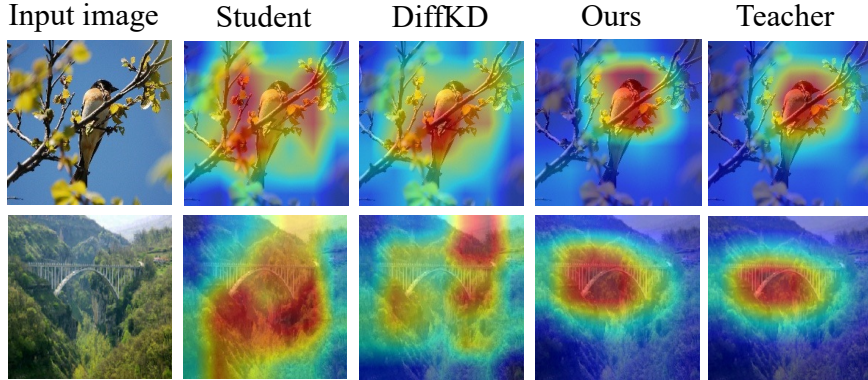


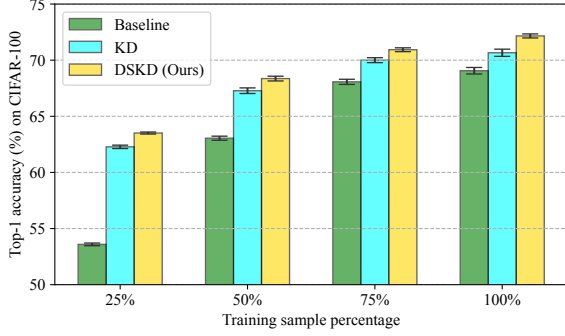
Figure 6 Visualizations of attention heatmaps generated by teacher as well as student trained by baseline, DiffKD and our DSKD on ImageNet.

4.10 Visualization of attention maps.

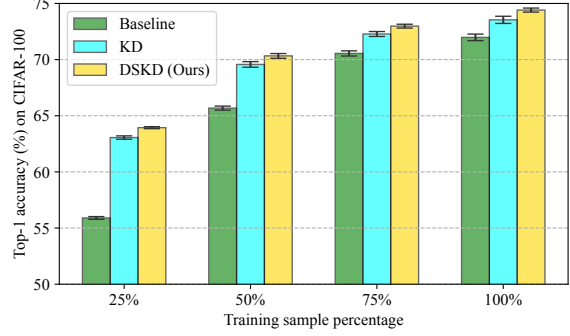
As shown in Figure 6, we visualize Grad-CAM [Selvaraju et al. \(2017\)](#) attention heatmaps generated by the teacher as well as the student trained by baseline, DiffKD, and our DSKD on ImageNet. We observed that our method learns more similar attention patterns and highlighted class-related features with the teacher. This enables the student to focus more precisely on target objects, further enhancing its performance. This can be attributed to *teacher-classifier-guided* diffusion model that improves the representational capability of student features.

4.11 Results on Few-Shot Scenario

In the real-world scenario, the training samples are often scarce. Therefore, we further examine the effectiveness of DSKD under few-shot scenario. As shown in Fig.7, we chooses 25%, 50%, and 75% training samples from the original training set for distillation, while reserving the original test set. For a fair comparison, we adopt a class-balanced data split strategy and retain the same data split results under a specific sample percentage across different distillation pairs. Our DSKD consistently outperforms Baseline and KD by 4.8% and 1.0% on average under few-shot scenarios, respectively. The traditional KD only forces the student to align class probability distributions to the teacher, leading to overfitting on the training set. By contrast, DSKD

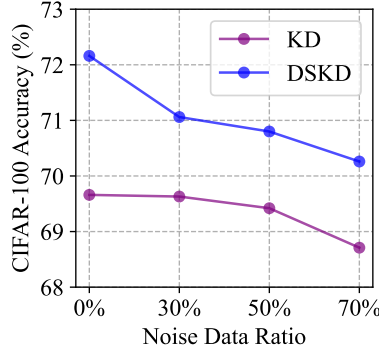


(a) ResNet-56 → ResNet-20

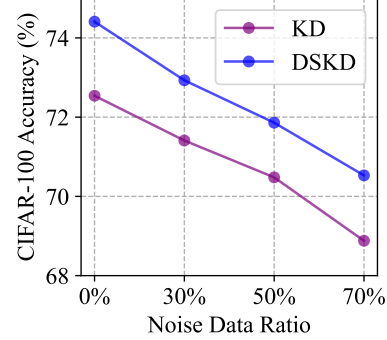


(b) WRN-40-2 → WRN-40-1

Figure 7 Top-1 accuracy (%) among Baseline, KD, and our DSKD under various training sample percentages.



(a) ResNet-56 → ResNet-20



(b) WRN-40-2 → WRN-40-1

Figure 8 Top-1 accuracy (%) among Baseline, KD, and our DSKD under various noise data ratios.

introduces diffusion model to assist feature distillation, making the student learn better feature representations and generalization capability.

4.12 Results on Noisy-Label Scenario

The real-world scenario often has many noise labels for model training. Therefore, we further verify the effectiveness of DSKD under noisy-label scenario. As shown in Fig.8, we disturb 30%, 50%, and 70% training samples with error labels, while reserving the original test set. We found that DSKD achieves better accuracy than KD across various noise data ratios. The results demonstrate that teacher-guided diffusion distillation makes the student learn more ground-truth knowledge from the teacher than highly relying on annotated labels. Such method augments the student's defend capability to label noise.

5 Conclusion

This paper proposes DSKD, a novel KD method by introducing teacher-classifier-guided diffusion model and performing student feature self-distillation to improve visual recognition tasks. Compared to previous methods, our DSKD avoids the teacher-student discrepancy problem and augments the student features with class-related information by the teacher classifier. Experimental results on image classification and semantic segmentation show that DSKD achieves the best performance. We hope this paper will inspire future research to explore advanced KD methods by introducing diffusion models.

References

Sungsoo Ahn, Shell Xu Hu, Andreas Damianou, Neil D Lawrence, and Zhenwen Dai. Variational information distillation for knowledge transfer. In *Proceedings of the IEEE/CVF Conference on Computer Vision and Pattern Recognition*, pages 9163–9171, 2019.

Liang-Chieh Chen, Yukun Zhu, George Papandreou, Florian Schroff, and Hartwig Adam. Encoder-decoder with atrous separable convolution for semantic image segmentation. In *Proceedings of the European conference on computer vision (ECCV)*, pages 801–818, 2018.

Pengguang Chen, Shu Liu, Hengshuang Zhao, and Jiaya Jia. Distilling knowledge via knowledge review. In *Proceedings of the IEEE/CVF Conference on Computer Vision and Pattern Recognition*, pages 5008–5017, 2021.

Jang Hyun Cho and Bharath Hariharan. On the efficacy of knowledge distillation. In *Proceedings of the IEEE/CVF international conference on computer vision*, pages 4794–4802, 2019.

Florinel-Alin Croitoru, Vlad Hondu, Radu Tudor Ionescu, and Mubarak Shah. Diffusion models in vision: A survey. *IEEE transactions on pattern analysis and machine intelligence*, 45(9):10850–10869, 2023.

Mayur Datar, Nicole Immorlica, Piotr Indyk, and Vahab S Mirrokni. Locality-sensitive hashing scheme based on p-stable distributions. In *Proceedings of the twentieth annual symposium on Computational geometry*, pages 253–262, 2004.

Jia Deng, Wei Dong, Richard Socher, Li-Jia Li, Kai Li, and Li Fei-Fei. Imagenet: A large-scale hierarchical image database. In *CVPR*, pages 248–255, 2009.

Prafulla Dhariwal and Alexander Nichol. Diffusion models beat gans on image synthesis. *Advances in neural information processing systems*, 34:8780–8794, 2021.

Jiawei Fan, Chao Li, Xiaolong Liu, Meina Song, and Anbang Yao. Augmentation-free dense contrastive knowledge distillation for efficient semantic segmentation. *Advances in Neural Information Processing Systems*, 36:51359–51370, 2023.

Weilun Feng, Chuanguang Yang, Zhulin An, Libo Huang, Boyu Diao, Fei Wang, and Yongjun Xu. Relational diffusion distillation for efficient image generation. In *Proceedings of the 32nd ACM international conference on multimedia*, pages 205–213, 2024.

Yingchao Feng, Xian Sun, Wenhui Diao, Jihao Li, and Xin Gao. Double similarity distillation for semantic image segmentation. *IEEE Transactions on Image Processing*, 30:5363–5376, 2021.

Ziying Guo, Haonan Yan, Hui Li, and Xiaodong Lin. Class attention transfer based knowledge distillation. In *Proceedings of the IEEE/CVF Conference on Computer Vision and Pattern Recognition*, pages 11868–11877, 2023.

Zhiwei Hao, Jianyuan Guo, Ding Jia, Kai Han, Yehui Tang, Chao Zhang, Han Hu, and Yunhe Wang. Learning efficient vision transformers via fine-grained manifold distillation. *Advances in Neural Information Processing Systems*, 35: 9164–9175, 2022.

Kaiming He, Xiangyu Zhang, Shaoqing Ren, and Jian Sun. Deep residual learning for image recognition. In *CVPR*, pages 770–778, 2016.

Geoffrey Hinton, Oriol Vinyals, and Jeff Dean. Distilling the knowledge in a neural network. *arXiv preprint arXiv:1503.02531*, 2015.

Jonathan Ho, Ajay Jain, and Pieter Abbeel. Denoising diffusion probabilistic models. *Advances in neural information processing systems*, 33:6840–6851, 2020.

Andrew Howard, Mark Sandler, Grace Chu, Liang-Chieh Chen, Bo Chen, Mingxing Tan, Weijun Wang, Yukun Zhu, Ruoming Pang, Vijay Vasudevan, et al. Searching for mobilenetv3. In *Proceedings of the IEEE/CVF international conference on computer vision*, pages 1314–1324, 2019.

Andrew G Howard, Menglong Zhu, Bo Chen, Dmitry Kalenichenko, Weijun Wang, Tobias Weyand, Marco Andreetto, and Hartwig Adam. Mobilenets: Efficient convolutional neural networks for mobile vision applications. *arXiv preprint arXiv:1704.04861*, 2017.

Tao Huang, Yuan Zhang, Mingkai Zheng, Shan You, Fei Wang, Chen Qian, and Chang Xu. Knowledge diffusion for distillation. *Advances in Neural Information Processing Systems*, 36:65299–65316, 2023.

Mingi Ji, Seungjae Shin, Seunghyun Hwang, Gibeom Park, and Il-Chul Moon. Refine myself by teaching myself: Feature refinement via self-knowledge distillation. In *Proceedings of the IEEE/CVF conference on computer vision and pattern recognition*, pages 10664–10673, 2021.

Kyungyul Kim, ByeongMoon Ji, Doyoung Yoon, and Sangheum Hwang. Self-knowledge distillation with progressive refinement of targets. In *Proceedings of the IEEE/CVF international conference on computer vision*, pages 6567–6576, 2021.

Alex Krizhevsky and Geoffrey Hinton. Learning multiple layers of features from tiny images. Technical report, Citeseer, 2009.

Zheng Li, Xiang Li, Lingfeng Yang, Borui Zhao, Renjie Song, Lei Luo, Jun Li, and Jian Yang. Curriculum temperature for knowledge distillation. In *Proceedings of the AAAI Conference on Artificial Intelligence*, volume 37, pages 1504–1512, 2023.

Tsung-Yi Lin, Michael Maire, Serge Belongie, James Hays, Pietro Perona, Deva Ramanan, Piotr Dollár, and C Lawrence Zitnick. Microsoft coco: Common objects in context. In *European conference on computer vision*, pages 740–755. Springer, 2014.

Tsung-Yi Lin, Priya Goyal, Ross Girshick, Kaiming He, and Piotr Dollár. Focal loss for dense object detection. In *Proceedings of the IEEE international conference on computer vision*, pages 2980–2988, 2017.

Tao Liu, Chenshu Chen, Xi Yang, and Wenming Tan. Rethinking knowledge distillation with raw features for semantic segmentation. In *Proceedings of the IEEE/CVF Winter Conference on Applications of Computer Vision*, pages 1155–1164, 2024.

Yifan Liu, Ke Chen, Chris Liu, Zengchang Qin, Zhenbo Luo, and Jingdong Wang. Structured knowledge distillation for semantic segmentation. In *Proceedings of the IEEE/CVF Conference on Computer Vision and Pattern Recognition*, pages 2604–2613, 2019.

Ze Liu, Yutong Lin, Yue Cao, Han Hu, Yixuan Wei, Zheng Zhang, Stephen Lin, and Baining Guo. Swin transformer: Hierarchical vision transformer using shifted windows. In *Proceedings of the IEEE/CVF international conference on computer vision*, pages 10012–10022, 2021.

Seyed Iman Mirzadeh, Mehrdad Farajtabar, Ang Li, Nir Levine, Akihiro Matsukawa, and Hassan Ghasemzadeh. Improved knowledge distillation via teacher assistant. In *Proceedings of the AAAI conference on artificial intelligence*, volume 34, pages 5191–5198, 2020.

Wonpyo Park, Dongju Kim, Yan Lu, and Minsu Cho. Relational knowledge distillation. In *Proceedings of the IEEE/CVF conference on computer vision and pattern recognition*, pages 3967–3976, 2019.

Nikolaos Passalis, Maria Tzelepi, and Anastasios Tefas. Probabilistic knowledge transfer for lightweight deep representation learning. *IEEE Transactions on Neural Networks and Learning Systems*, 32(5):2030–2039, 2020.

William Peebles and Saining Xie. Scalable diffusion models with transformers. In *Proceedings of the IEEE/CVF international conference on computer vision*, pages 4195–4205, 2023.

Cuong Pham, Van-Anh Nguyen, Trung Le, Dinh Phung, Gustavo Carneiro, and Thanh-Toan Do. Frequency attention for knowledge distillation. In *Proceedings of the IEEE/CVF Winter Conference on Applications of Computer Vision*, pages 2277–2286, 2024.

Shaoqing Ren, Kaiming He, Ross Girshick, and Jian Sun. Faster r-cnn: Towards real-time object detection with region proposal networks. *Advances in neural information processing systems*, 28, 2015.

Adriana Romero, Nicolas Ballas, Samira Ebrahimi Kahou, Antoine Chassang, Carlo Gatta, and Yoshua Bengio. Fitnets: Hints for thin deep nets. *arXiv preprint arXiv:1412.6550*, 2014.

Olaf Ronneberger, Philipp Fischer, and Thomas Brox. U-net: Convolutional networks for biomedical image segmentation. In *International Conference on Medical image computing and computer-assisted intervention*, pages 234–241. Springer, 2015.

Tim Salimans and Jonathan Ho. Progressive distillation for fast sampling of diffusion models. *arXiv preprint arXiv:2202.00512*, 2022.

Ramprasaath R Selvaraju, Michael Cogswell, Abhishek Das, Ramakrishna Vedantam, Devi Parikh, and Dhruv Batra. Grad-cam: Visual explanations from deep networks via gradient-based localization. In *Proceedings of the IEEE international conference on computer vision*, pages 618–626, 2017.

Yiqing Shen, Liwu Xu, Yuzhe Yang, Yaqian Li, and Yandong Guo. Self-distillation from the last mini-batch for consistency regularization. In *Proceedings of the IEEE/CVF conference on computer vision and pattern recognition*, pages 11943–11952, 2022.

Changyong Shu, Yifan Liu, Jianfei Gao, Zheng Yan, and Chunhua Shen. Channel-wise knowledge distillation for dense prediction. In *Proceedings of the IEEE/CVF International Conference on Computer Vision*, pages 5311–5320, 2021.

Jiaming Song, Chenlin Meng, and Stefano Ermon. Denoising diffusion implicit models. *arXiv preprint arXiv:2010.02502*, 2020.

Shangquan Sun, Wenqi Ren, Jingzhi Li, Rui Wang, and Xiaochun Cao. Logit standardization in knowledge distillation. In *Proceedings of the IEEE/CVF Conference on Computer Vision and Pattern Recognition*, pages 15731–15740, 2024.

Wujie Sun, Defang Chen, Can Wang, Deshi Ye, Yan Feng, and Chun Chen. Accelerating diffusion sampling with classifier-based feature distillation. In *2023 IEEE International Conference on Multimedia and Expo (ICME)*, pages 810–815. IEEE, 2023.

Wujie Sun, Defang Chen, Siwei Lyu, Genlang Chen, Chun Chen, and Can Wang. Knowledge distillation with refined logits. In *Proceedings of the IEEE/CVF International Conference on Computer Vision*, pages 1110–1119, 2025.

Yonglong Tian, Dilip Krishnan, and Phillip Isola. Contrastive representation distillation. *arXiv preprint arXiv:1910.10699*, 2019a.

Zhi Tian, Chunhua Shen, Hao Chen, and Tong He. Fcos: Fully convolutional one-stage object detection. In *Proceedings of the IEEE/CVF international conference on computer vision*, pages 9627–9636, 2019b.

Zhuotao Tian, Pengguang Chen, Xin Lai, Li Jiang, Shu Liu, Hengshuang Zhao, Bei Yu, Ming-Chang Yang, and Jiaya Jia. Adaptive perspective distillation for semantic segmentation. *IEEE Transactions on Pattern Analysis and Machine Intelligence*, 45(2):1372–1387, 2022.

Guo-Hua Wang, Yifan Ge, and Jianxin Wu. Distilling knowledge by mimicking features. *IEEE Transactions on Pattern Analysis and Machine Intelligence*, 44(11):8183–8195, 2021.

Lu Wang, Liuchi Xu, Xiong Yang, Zhenhua Huang, and Jun Cheng. Debiased distillation for consistency regularization. In *Proceedings of the AAAI Conference on Artificial Intelligence*, volume 39, pages 7799–7807, 2025.

Yukang Wang, Wei Zhou, Tao Jiang, Xiang Bai, and Yongchao Xu. Intra-class feature variation distillation for semantic segmentation. In *European Conference on Computer Vision*, pages 346–362. Springer, 2020.

Shicai Wei, Chunbo Luo, and Yang Luo. Scaled decoupled distillation. In *Proceedings of the IEEE/CVF Conference on Computer Vision and Pattern Recognition*, pages 15975–15983, 2024.

Kai Xu, Lichun Wang, Shuang Li, Jianjia Xin, and Baocai Yin. Self-distillation with augmentation in feature space. *IEEE Transactions on Circuits and Systems for Video Technology*, 34(10):9578–9590, 2024.

Kunran Xu, Lai Rui, Yishi Li, and Lin Gu. Feature normalized knowledge distillation for image classification. In *European conference on computer vision*, pages 664–680. Springer, 2020.

Chuanguang Yang, Zhulin An, Linhang Cai, and Yongjun Xu. Hierarchical self-supervised augmented knowledge distillation. In *Proceedings of the Thirtieth International Joint Conference on Artificial Intelligence*, pages 1217–1223, 2021.

Chuanguang Yang, Zhulin An, Helong Zhou, Linhang Cai, Xiang Zhi, Jiwen Wu, Yongjun Xu, and Qian Zhang. Mixskd: Self-knowledge distillation from mixup for image recognition. In *European Conference on Computer Vision*, pages 534–551. Springer, 2022a.

Chuanguang Yang, Helong Zhou, Zhulin An, Xue Jiang, Yongjun Xu, and Qian Zhang. Cross-image relational knowledge distillation for semantic segmentation. In *Proceedings of the IEEE/CVF Conference on Computer Vision and Pattern Recognition*, pages 12319–12328, 2022b.

Chuanguang Yang, Zhulin An, Helong Zhou, Fuzhen Zhuang, Yongjun Xu, and Qian Zhang. Online knowledge distillation via mutual contrastive learning for visual recognition. *IEEE Transactions on Pattern Analysis and Machine Intelligence*, 45(8):10212–10227, 2023.

Li Yuan, Francis EH Tay, Guilin Li, Tao Wang, and Jiashi Feng. Revisiting knowledge distillation via label smoothing regularization. In *Proceedings of the IEEE/CVF conference on computer vision and pattern recognition*, pages 3903–3911, 2020.

Sukmin Yun, Jongjin Park, Kimin Lee, and Jinwoo Shin. Regularizing class-wise predictions via self-knowledge distillation. In *Proceedings of the IEEE/CVF conference on computer vision and pattern recognition*, pages 13876–13885, 2020.

Sergey Zagoruyko and Nikos Komodakis. Paying more attention to attention: Improving the performance of convolutional neural networks via attention transfer. *arXiv preprint arXiv:1612.03928*, 2016.

Komodakis N Zagoruyko S. Wide residual networks. In *Proceedings of the British Machine Vision Conference*, 2016.

Linfeng Zhang, Jiebo Song, Anni Gao, Jingwei Chen, Chenglong Bao, and Kaisheng Ma. Be your own teacher: Improve the performance of convolutional neural networks via self distillation. In *Proceedings of the IEEE/CVF international conference on computer vision*, pages 3713–3722, 2019.

Borui Zhao, Quan Cui, Renjie Song, Yiyu Qiu, and Jiajun Liang. Decoupled knowledge distillation. In *Proceedings of the IEEE/CVF Conference on computer vision and pattern recognition*, pages 11953–11962, 2022.

Bolei Zhou, Hang Zhao, Xavier Puig, Sanja Fidler, Adela Barriuso, and Antonio Torralba. Scene parsing through ade20k dataset. In *Proceedings of the IEEE conference on computer vision and pattern recognition*, pages 633–641, 2017.

Jinguo Zhu, Shixiang Tang, Dapeng Chen, Shijie Yu, Yakun Liu, Mingzhe Rong, Aijun Yang, and Xiaohua Wang. Complementary relation contrastive distillation. In *Proceedings of the IEEE/CVF conference on computer vision and pattern recognition*, pages 9260–9269, 2021.

Appendix

A Methodology

A.1 Teacher-Guided Student Feature Denoising

Inspired by the work *classifier-guided diffusion model* Dhariwal and Nichol (2021), we designed a new feature distillation method by using the teacher model to guide the reverse denoising process of the student features. Under the teacher’s guidance, the distribution of the student features shifts towards that of the teacher features, enriching the student features with meaningful semantic information from the teacher.

The denoising process of classifier-guided diffusion model Dhariwal and Nichol (2021) is formulated as:

$$p_{\theta, \phi}(\mathbf{x}_t | \mathbf{x}_{t+1}, y) = Z p_{\theta}(\mathbf{x}_t | \mathbf{x}_{t+1}) p_{\phi}(y | \mathbf{x}_t). \quad (17)$$

Here, the definition of each variable follows the original paper Dhariwal and Nichol (2021). Z is a normalizing constant, $p_{\theta}(\mathbf{x}_t | \mathbf{x}_{t+1})$ is an unconditional reverse noising process following DDPM Ho et al. (2020), and $p_{\phi}(y | \mathbf{x}_t)$ is a classifier, where \mathbf{x}_t is the noise image at the t -th step, and y is a class label.

In the context of teacher-student distillation, we formulate $p_{\phi}(y | \mathbf{x}_t)$ as the pre-trained teacher classifier, and \mathbf{x}_t as the denoised student features at the t -th step. Unlike the traditional denoising formula, we condition the sampling process on the student features $\mathbf{f}^{(stu)} \in \mathbb{R}^{H \times W \times D}$, where H , W , and C represent height, width, and the number of channels, respectively. We start $\mathbf{f}^{(stu)}$ as \mathbf{x}_T to perform teacher-guided diffusion sampling by T steps, *i.e.* $t = T, \dots, 2, 1$. \mathbf{x}_t denotes the denoised student features at the t -th time step. Therefore, the sampling formula of Equ.(17) can be expressed as follows:

$$p(\mathbf{x}_t | \mathbf{x}_{t+1}, y; \boldsymbol{\theta}, \boldsymbol{\phi}^{(tea)}) = Z p_{\boldsymbol{\theta}}(\mathbf{x}_t | \mathbf{x}_{t+1}) p(y | \mathbf{x}_t; \boldsymbol{\phi}^{(tea)}). \quad (18)$$

$p(\mathbf{x}_t | \mathbf{x}_{t+1}, y; \boldsymbol{\theta}, \boldsymbol{\phi}^{(tea)})$ is a conditional Markov process to denoised the student feature from \mathbf{x}_{t+1} to \mathbf{x}_t , conditioned by the noise predictor $\boldsymbol{\theta}$ and the teacher classifier $\boldsymbol{\phi}^{(tea)}$. $p(y | \mathbf{x}_t; \boldsymbol{\phi}^{(tea)})$ is the conditional probability of the predicted class y based on the student features \mathbf{x}_t inferred from the teacher classifier $\boldsymbol{\phi}^{(tea)}$. The teacher classifier often includes a global average pooling layer and a linear weight matrix to output class probability distribution. We adopt the traditional diffusion model that predicts \mathbf{x}_t from \mathbf{x}_{t+1} according to a Gaussian distribution:

$$p_{\boldsymbol{\theta}}(\mathbf{x}_t | \mathbf{x}_{t+1}) = \mathcal{N}(\boldsymbol{\mu}, \boldsymbol{\Sigma}), \quad (19)$$

where $\boldsymbol{\mu} = \boldsymbol{\mu}_{\boldsymbol{\theta}}(\mathbf{x}_{t+1})$, $\boldsymbol{\Sigma} = \boldsymbol{\Sigma}_{\boldsymbol{\theta}}(\mathbf{x}_{t+1})$. The logarithm form of Equ.(19) is formulated as:

$$\log p_{\boldsymbol{\theta}}(\mathbf{x}_t | \mathbf{x}_{t+1}) = -\frac{1}{2}(\mathbf{x}_t - \boldsymbol{\mu})^\top \boldsymbol{\Sigma}^{-1}(\mathbf{x}_t - \boldsymbol{\mu}) + C. \quad (20)$$

When the number of diffusion steps is limited to be infinite, we can derive $\|\boldsymbol{\Sigma}\| \rightarrow \mathbf{0}$. In this case, $p(y | \mathbf{x}_t; \boldsymbol{\phi}^{(tea)})$ has low curvature compared to $\boldsymbol{\Sigma}^{-1}$. Therefore, we can approximate $\log p(y | \mathbf{x}_t; \boldsymbol{\phi}^{(tea)})$ by a first-order Taylor expansion at $\mathbf{x}_t = \boldsymbol{\mu}$:

$$\begin{aligned} \log p(y | \mathbf{x}_t; \boldsymbol{\phi}^{(tea)}) &\approx \log p(y | \mathbf{x}_t; \boldsymbol{\phi}^{(tea)})|_{\mathbf{x}_t=\boldsymbol{\mu}} \\ &+ (\mathbf{x}_t - \boldsymbol{\mu}) \bigtriangledown_{\mathbf{x}_t} \log p(y | \mathbf{x}_t; \boldsymbol{\phi}^{(tea)})|_{\mathbf{x}_t=\boldsymbol{\mu}} \\ &= (\mathbf{x}_t - \boldsymbol{\mu}) \mathbf{g} + C_1, \end{aligned} \quad (21)$$

where $\mathbf{g} = \bigtriangledown_{\mathbf{x}_t} \log p(y | \mathbf{x}_t; \boldsymbol{\phi}^{(tea)})|_{\mathbf{x}_t=\boldsymbol{\mu}}$, and C_1 can be regarded as a constant. We can further derive the logarithm form of Equ.(18) as:

$$\begin{aligned} &\log(p_{\boldsymbol{\theta}}(\mathbf{x}_t | \mathbf{x}_{t+1}) p(y | \mathbf{x}_t; \boldsymbol{\phi}^{(tea)})) \\ &\approx -\frac{1}{2}(\mathbf{x}_t - \boldsymbol{\mu})^\top \boldsymbol{\Sigma}^{-1}(\mathbf{x}_t - \boldsymbol{\mu}) + (\mathbf{x}_t - \boldsymbol{\mu}) \mathbf{g} + C_2 \\ &= -\frac{1}{2}(\mathbf{x}_t - \boldsymbol{\mu} - \boldsymbol{\Sigma} \mathbf{g})^\top \boldsymbol{\Sigma}^{-1}(\mathbf{x}_t - \boldsymbol{\mu} - \boldsymbol{\Sigma} \mathbf{g}) + \frac{1}{2} \mathbf{g}^\top \boldsymbol{\Sigma} \mathbf{g} + C_2 \\ &= -\frac{1}{2}(\mathbf{x}_t - \boldsymbol{\mu} - \boldsymbol{\Sigma} \mathbf{g})^\top \boldsymbol{\Sigma}^{-1}(\mathbf{x}_t - \boldsymbol{\mu} - \boldsymbol{\Sigma} \mathbf{g}) + C_3 \\ &= \log p(\mathbf{z}) + C_4, \end{aligned} \quad (22)$$

where $\mathbf{z} \sim \mathcal{N}(\boldsymbol{\mu} + \boldsymbol{\Sigma}\mathbf{g}, \boldsymbol{\Sigma})$. The detailed proof is shown in Appendix A.1. Therefore, the conditional sampling strategy can be approximated to the unconditional Gaussian sampling, but differs in the shifted mean by $\boldsymbol{\Sigma}\mathbf{g}$. Moreover, we introduce a gradient scale k as the guidance strength over the gradient of the teacher classifier. In summary, the teacher-guided diffusion sampling is formulated as:

$$\mathbf{x}_{t-1} \sim \mathcal{N}(\boldsymbol{\mu} + k\boldsymbol{\Sigma} \nabla_{\mathbf{x}_t} \log p(y|\mathbf{x}_t; \boldsymbol{\phi}^{(tea)}), \boldsymbol{\Sigma}). \quad (23)$$

In theory, the gradient scale k can smooth the teacher class probability distribution, proportional to $p(y|\mathbf{x}_t; \boldsymbol{\phi}^{(tea)})^k$. When $k > 1$, the distribution becomes sharper, meaning that the teacher classifier has stronger guidance strength, resulting in higher fidelity (but less diverse) image features.

After the teacher-guided diffusion sampling process proceeds by T steps, the original student features $\mathbf{f}^{(stu)}$ (*i.e.* \mathbf{x}_T) is converted to the denoised student features $\hat{\mathbf{f}}^{(stu)}$ (*i.e.* \mathbf{x}_0).

A.2 Details of Noise Adapter

Consistent with our previous discussion, we model the student feature as a noisy approximation of the teacher. However, the magnitude of this noise—reflecting the discrepancy between the two—is latent and varies across different training instances. This variability precludes the direct identification of the optimal initial diffusion timestep. To overcome this hurdle, we propose an adaptive noise matching module designed to calibrate the student feature’s noise intensity to a pre-determined level.

We employ a lightweight convolutional block to regress a mixing coefficient κ , which blends the student output with Gaussian noise. This operation is designed to calibrate the student’s noise magnitude to match the specific intensity required at the initial timestep T . Consequently, the starting feature for the denoising trajectory is formulated as:

$$\hat{\mathbf{f}}_T^{(stu)} = \kappa \mathbf{f}^{(stu)} + (1 - \kappa) \boldsymbol{\epsilon}_T. \quad (24)$$

The optimization of this noise calibration is inherently driven by the KD objective. This is predicated on the fact that achieving the lowest discrepancy between the denoised student and the teacher requires the student to be precisely aligned with the target noise intensity during the denoising phase.